Eur. Phys. J. B (2018) 91: 132
https://doi.org/10.1140/epjb/e2018-90070-4

THE EUROPEAN PHYSICAL JOURNAL B

Regular Article

Ballistic transport in aperiodic Labyrinth tiling proven through a new convolution theorem

Fernando Sánchez[1], Vicenta Sánchez[1], and Chumin Wang[2,a]

[1] Departamento de Física, Facultad de Ciencias, Universidad Nacional Autónoma de México, 04510 Ciudad de México, Mexico
[2] Instituto de Investigaciones en Materiales, Universidad Nacional Autónoma de México, 04510 Ciudad de México, Mexico

Received 11 February 2018 / Received in final form 18 April 2018
Published online 27 June 2018

Abstract. In this article, we report a distinct convolution theorem developed for the Kubo-Greenwood formula in Labyrinth tiling by transforming the two-dimensional lattice into a set of independent chains with rescaled Hamiltonians. Such transformation leads to an analytical solution of the direct-current conductance spectra, where quantized steps with height of $2g_0$ are found in Labyrinth tiling with periodic order along the applied electric field direction, in contrast to the step height of g_0 observed in the corresponding square lattices, being g_0 the conductance quantum. When this convolution theorem is combined with the real-space renormalization method, we are able to address in non-perturbative way the electronic transport in macroscopic aperiodic Labyrinth tiling based on generalized Fibonacci chains. Furthermore, we analytically demonstrate the existence of ballistic transport states in aperiodic Labyrinth tiling. This finding suggests that the periodicity should not be a necessary condition for the single-electron ballistic transport even in multidimensional fully non-periodic lattices.

1 Introduction

The search for a simple and direct relationship between atomic scale arrangement and macroscopic properties of a material constitutes a principal task of the materials science. For example, the Bloch theorem establishes extended electronic wavefunctions and then a ballistic conduction if the atoms of a crystal are periodically ordered [1]. At the other extreme, for an amorphous solid with randomly arranged atoms, the scaling analysis indicates only exponentially localized eigenstates in one-dimensional (1D) and two-dimensional (2D) systems [2]. There is a wide range of structural disorders in between, such as the quasicrystals discovered by D. Shechtman in 1984 [3], which possess a long range rotational order without periodicity. Based on the Lebesgue's decomposition theorem, aperiodic systems can be classified through its lattice Fourier transform spectrum in three different types: pure-point, as revealed by the electron diffraction pattern of quasicrystals [3], singular-continuous and absolutely-continuous spectra [4,5]. It has been demonstrated that the Fourier transform spectrum of a periodic or aperiodic binary lattice is discrete, if the eigenvalues of its substitutional matrix obtained from the irreducible Pisot polynomial satisfy the Pisot-Vijayaraghavan (PV) condition [6,7]. Moreover, within the tight-binding formalism, the electronic wavefunctions of 1D quasiperiodic systems have been proven to be critical [8] with power law localization [9] and the corresponding eigenvalue spectrum is a Cantor set with zero-Lebesgue measure [10]. In general, this formalism has the advantage of being simple and capable to reproduce experimental data, since many-body effects are partially considered through its semi-empirical parameters. Furthermore, such simplicity permits isolate the structural disorder effects on the electronic transport in quasiperiodic systems. Hence, the tight-binding approach is nowadays being extensively used for the understanding of new physical phenomena occurred in a wide range of aperiodic systems [4,11,12].

In general, eigenmodes in 1D aperiodic systems may exhibit a localization-delocalization transition, but such transition is not guaranteed in higher dimensional ones [13], whose spectral and transport properties remain as unsolved problems. In the past, most studies of 2D aperiodic systems were carried out for thousands of atoms [14] or through the perturbation theory [15,16]. However, the former is unsuitable to analyze the long range quasiperiodic effects, while the latter cannot address high contrast aperiodic systems. For the case of tight-binding model, the off-diagonal aperiodic Hamiltonian of cubic-type lattices is separable [17] and may be written as a sum of Euclidean products of 1D systems [18].

Beyond these cubic-type multidimensional aperiodic lattices, an interesting alternative could be the connection

[a] e-mail: chumin@unam.mx

of second neighbors in the square Fibonacci lattice, called Labyrinth tiling [19], i.e., a 2D rhombic lattice with non-constant bond lengths built by the Euclidean product of two 1D aperiodic ones [20–22]. In this article, we report a new convolution theorem for separable tight-binding Hamiltonians expressed as a product of individual ones, in contrast to the previous one developed for Hamiltonians expressed as a sum of them [18]. This convolution theorem combined with the real-space renormalization method allows to analyze the electronic transport in macroscopic multidimensional Labyrinth tiling.

This paper is organized as follows: in Section 2 we introduce 2D Labyrinth tiling and its tight-binding Hamiltonian through the product of those from two linear chains. We further demonstrate in Section 3 a distinct convolution theorem for the density of states (DOS) and a detailed proof of such theorem for the Kubo-Greenwood formula is given in Appendix A. The obtained DOS of silver-mean Labyrinth tiling is compared with those reported in the literature. In Section 4, we study the electrical conductance of 2D Labyrinth tiling based on generalized Fibonacci (GF) chains by combining the convolution theorem with a previously developed real-space renormalization method. In addition, an unusual ballistic conduction state is found at the center of several conductance spectra and its existence in such multidimensional Labyrinth tilings is analytically proven in Section 5. Finally, some conclusive remarks are presented in Section 6.

2 Labyrinth tiling

A 2D aperiodic Labyrinth tiling can be obtained from the Euclidean product of two 1D aperiodic chains [23], such as the Fibonacci one constructed by using two unequal building blocks A and B through the substitution rule of $A \to AB$ and $B \to A$. A GF lattice may be obtained by following a general substitution rule given by $A \to A^m B^n$ and $B \to A$ where $m, n \in \mathbb{Z}^+$ [24,25]. There are several isomers for each (m,n)-type GF lattice and they obey the rules $A \to A^m B^n$, $A \to A^{m-1}BAB^{n-1}, \ldots, A \to B^n A^m$. These isomers possess almost the same DOS, but different transport properties [26]. Moreover, the GF lattices with $m > 1$ and $n = 1$ are called precious means, whose substitution matrix satisfies the PV conditions. Thus, they are quasiperiodic systems [27]. For metallic means with $m = 1$ and $n > 1$, these conditions are not fulfilled and then their lattice Fourier transform spectrum does not consist of pure points since they are not quasiperiodic lattices [7].

In order to study the electronic transport in aperiodic lattices, we start from a 1D nearest-neighbor single-band tight-binding Hamiltonian ($\hat{H}^{1D}$), which can be written as

$$\hat{H}^{1D} = \sum_i \left(t_{i,i+1} |i\rangle\langle i+1| + t_{i,i-1} |i\rangle\langle i-1| \right), \qquad (1)$$

where $|i\rangle$ represents the Wannier function at atom i with null self-energy and $t_{i,i\pm1}$ are the hopping integrals between nearest-neighbor sites i and $i \pm 1$, whose values can be t_A or t_B ordered following the GF sequences. A coupling constant,

$$\lambda \equiv |t_A^2 - t_B^2| / t_A t_B, \qquad (2)$$

can be introduced to quantify the disorder strength [28].

From two 1D Hamiltonians of equation (1), it is possible to construct 2D ones. For example, $\hat{H}^{2D}_{sq} = \hat{H}^{1D}_x \otimes \hat{I}_y + \hat{I}_x \otimes \hat{H}^{1D}_y$ is the Hamiltonian of a square lattice, where $\hat{I}_\kappa$ is the 1D identity operator with $\kappa = x$ or y. The energy spectrum of $\hat{H}^{2D}_{sq}$ is given by $E^{2D}_{sq} = E^{1D}_x + E^{1D}_y$, being E^{1D}_κ the energy spectrum of $\hat{H}^{1D}_\kappa$. This spectrum is an interval if parameters λ_x and λ_y defined in equation (2) are sufficiently close to zero, and it is a Cantor set of zero Lebesgue measure if λ_x and λ_y are large enough [28].

A more general 2D Hamiltonian, through the Euclidean product ($\otimes$) between two 1D-Hamiltonians, can be written as [19]

$$\begin{aligned}\hat{H}^{2D} &= \frac{1}{V}\left(\hat{H}^{\parallel} + \varepsilon_{\parallel} I_{\parallel}\right) \otimes \left(\hat{H}^{\perp} + \varepsilon_{\perp} I_{\perp}\right) \\ &= \frac{1}{V} \sum_{i,k} \begin{pmatrix} \varepsilon_{\parallel}\varepsilon_{\perp} |i,k\rangle\langle i,k| \\ +\varepsilon_{\perp} t_{i,i+1} |i,k\rangle\langle i+1,k| \\ +\varepsilon_{\perp} t_{i,i-1} |i,k\rangle\langle i-1,k| \\ +\varepsilon_{\parallel} t_{k,k+1} |i,k\rangle\langle i,k+1| \\ +\varepsilon_{\parallel} t_{k,k-1} |i,k\rangle\langle i,k-1| \\ +t_{k,k+1} t_{i,i+1} |i,k\rangle\langle i+1,k+1| \\ +t_{k,k+1} t_{i,i-1} |i,k\rangle\langle i-1,k+1| \\ +t_{k,k-1} t_{i,i+1} |i,k\rangle\langle i+1,k-1| \\ +t_{k,k-1} t_{i,i-1} |i,k\rangle\langle i-1,k-1| \end{pmatrix}, \end{aligned} \qquad (3)$$

where V is an energy scale parameter, $\hat{H}^{\parallel}$ and $\hat{H}^{\perp}$ are respectively 1D Hamiltonians of equation (1) along the parallel and perpendicular directions respect to the applied electric field, $\varepsilon_{\parallel}$ and $\varepsilon_{\perp}$ are correspondingly the self-energies of atoms in parallel and perpendicular subspace, and $|i,k\rangle = |i\rangle|k\rangle$, being $|i\rangle$ and $|k\rangle$ Wannier functions in the parallel and perpendicular subspace, respectively. Hence, the 2D energy spectrum is given by

$$E^{2D}_{\alpha,\beta} = \frac{1}{V}(E^{\parallel}_{\alpha} + \varepsilon_{\parallel})(E^{\perp}_{\beta} + \varepsilon_{\perp}), \qquad (4)$$

where $\hat{H}^{2D}|\alpha,\beta\rangle = E^{2D}_{\alpha,\beta}|\alpha,\beta\rangle$, $\hat{H}^{\parallel}|\alpha\rangle = E^{\parallel}_{\alpha}|\alpha\rangle$ and $\hat{H}^{\perp}|\beta\rangle = E^{\perp}_{\beta}|\beta\rangle$. Therefore, from equations (3) and (4) we have

$$\begin{aligned} &\frac{1}{V}\sum_{i,k} \begin{pmatrix} \varepsilon_{\parallel} t_{k,k+1} |i,k\rangle\langle i,k+1| \\ +t_{k,k+1} t_{i,i+1} |i,k\rangle\langle i+1,k+1| \\ +\varepsilon_{\parallel} t_{k,k-1} |i,k\rangle\langle i,k-1| \\ +t_{k,k-1} t_{i,i-1} |i,k\rangle\langle i-1,k-1| \\ +\varepsilon_{\perp} t_{i,i+1} |i,k\rangle\langle i+1,k| \\ +t_{k,k-1} t_{i,i+1} |i,k\rangle\langle i+1,k-1| \\ +\varepsilon_{\perp} t_{i,i-1} |i,k\rangle\langle i-1,k| \\ +t_{k,k+1} t_{i,i-1} |i,k\rangle\langle i-1,k+1| \end{pmatrix} |\alpha,\beta\rangle \\ &= \frac{(E^{\parallel}_{\alpha} + \varepsilon_{\parallel})(E^{\perp}_{\beta} + \varepsilon_{\perp}) - \varepsilon_{\parallel}\varepsilon_{\perp}}{V} |\alpha,\beta\rangle. \end{aligned} \qquad (5)$$

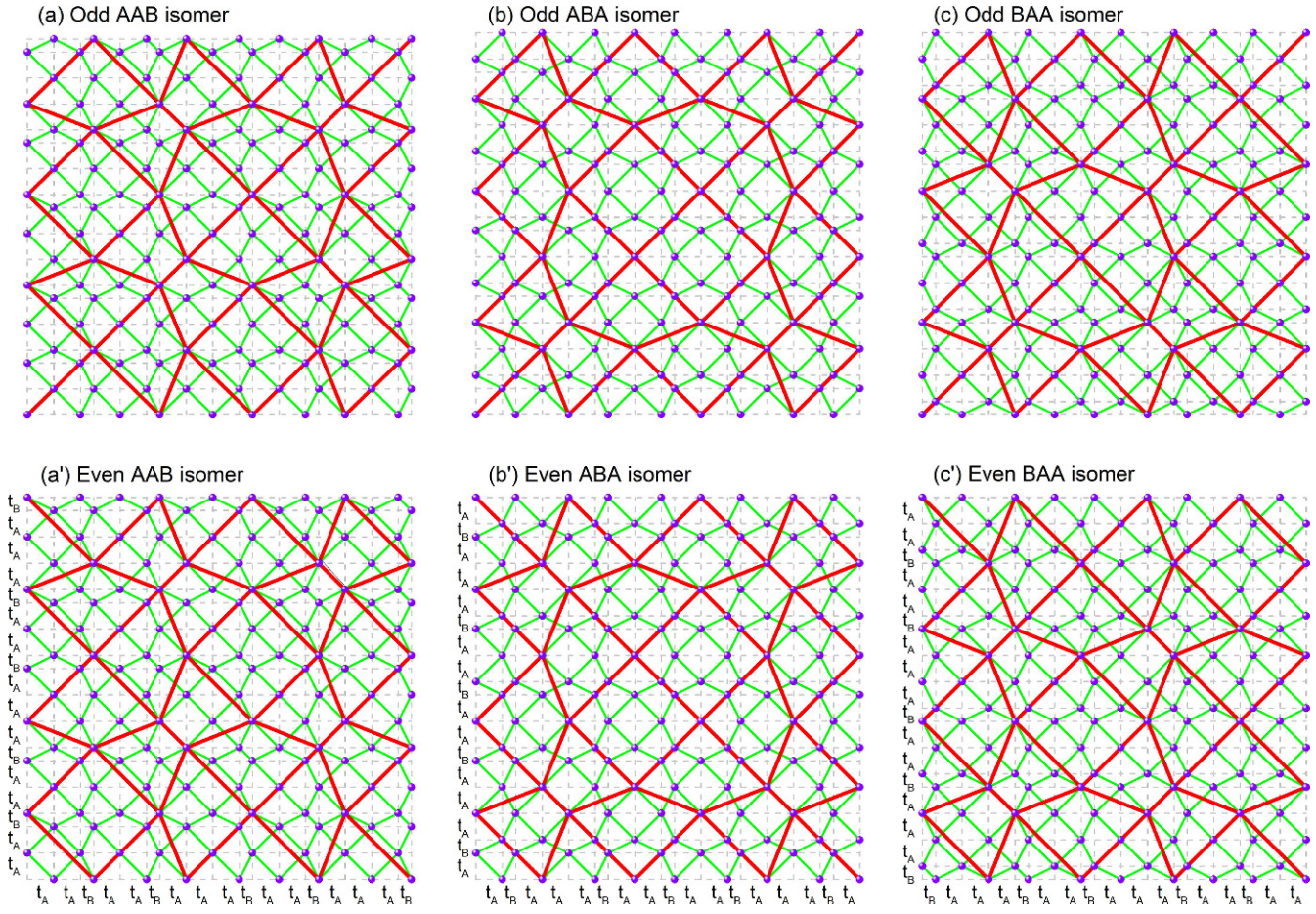

Fig. 1. Labyrinth tiling (green lines), based on a 2D silver mean lattice (gray dashed lines), for (a,a′) AAB, (b,b′) ABA and (c,c′) BAA isomers with (a–c) odd or (a′–c′) even options. The red thick lines illustrate the scale invariance of Labyrinth tiling.

For the limiting case of $\varepsilon_{\parallel} = \varepsilon_{\perp} = V$ and $V \to \infty$, equation (5) reduces to

$$\hat{H}_{Sq}^{2D}|\alpha,\beta\rangle = \sum_{i,k} \begin{pmatrix} t_{k,k+1}|i,k\rangle\langle i,k+1| \\ +t_{k,k-1}|i,k\rangle\langle i,k-1| \\ +t_{i,i+1}|i,k\rangle\langle i+1,k| \\ +t_{i,i-1}|i,k\rangle\langle i-1,k| \end{pmatrix} |\alpha,\beta\rangle$$
$$= (E_{\alpha}^{\parallel} + E_{\beta}^{\perp})|\alpha,\beta\rangle, \quad (6)$$

which corresponds to the Schrödinger equation of a square lattice. On the other hand, for the opposite limiting case of $\varepsilon_{\parallel} = \varepsilon_{\perp} = 0$, equation (5) can be rewritten as [29]

$$\hat{H}_{Lb}^{2D}|\alpha,\beta\rangle = \frac{1}{V}\sum_{i,k} \begin{pmatrix} t_{k,k+1}t_{i,i+1}|i,k\rangle\langle i+1,k+1| \\ +t_{k,k-1}t_{i,i-1}|i,k\rangle\langle i-1,k-1| \\ +t_{k,k-1}t_{i,i+1}|i,k\rangle\langle i+1,k-1| \\ +t_{k,k+1}t_{i,i-1}|i,k\rangle\langle i-1,k+1| \end{pmatrix} |\alpha,\beta\rangle$$
$$= \frac{E_{\alpha}^{\parallel}E_{\beta}^{\perp}}{V}|\alpha,\beta\rangle, \quad (7)$$

which corresponds to the Schrödinger equation of a Labyrinth tiling, as shown in Figure 1 for the case of silver-mean sequence along both parallel and perpendicular directions. The energy spectrum of the Labyrinth tiling is an interval if parameters λ_x and λ_y defined in equation (2) are sufficiently close to zero, and it is a Cantor set of zero Lebesgue measure if λ_x and λ_y are large enough, as occurred in the square lattice [30]. From equation (7), the hopping integral between atoms with Cartesian coordinates (j,k) and $(j+1,k+1)$ in a 2D Labyrinth tiling is given by

$$t_{(j,k)(j+1,k+1)} = \langle j,k|\hat{H}_{Lb}^{2D}|j+1,k+1\rangle$$
$$= \frac{1}{V}\sum_{l,r}\langle j,k|\hat{H}^{\parallel}|l,r\rangle\langle l,r|\hat{H}^{\perp}|j+1,k+1\rangle,$$
$$= \frac{1}{V}\left(t_{(j,k)(j+1,k)}t_{(j+1,k)(j+1,k+1)} + t_{(j,k)(j,k+1)}t_{(j,k+1)(j+1,k+1)}\right), \quad (8)$$

since $\hat{H}^{\parallel}$ and $\hat{H}^{\perp}$ only consider nearest-neighbor hopping processes.

Figure 1 shows the scaling property, illustrated by green thin and red thick lines, of Labyrinth tiling based on the silver mean sequence $(m=2, n=1)$ of generation 4 (gray dashed lines), for (a–c) odd and (a′–c′) even Labyrinth tiling corresponding to (a,a′) AAB, (b,b′) ABA and (c,c′) BAA isomers. This scaling property can be visualized by using three different 2D building units (O, P, Q) and for a

silver-mean Labyrinth tiling, they are shown in Figure 2 including their respective 2D substitution rules, which for a Labyrinth tiling based on (m,n)-type GF can be written as

$$\begin{pmatrix} O \\ P \\ Q \end{pmatrix} \rightarrow \mathbf{W} \begin{pmatrix} O \\ P \\ Q \end{pmatrix} = \begin{pmatrix} m^2 & n^2 & 2mn \\ 1 & 0 & 0 \\ m & 0 & n \end{pmatrix} \begin{pmatrix} O \\ P \\ Q \end{pmatrix}. \tag{9}$$

Eigenvalues (ξ) of the substitution matrix $(\mathbf{W})$ are roots of

$$\begin{aligned} \det(\mathbf{W} - \xi\mathbf{I}) &= \begin{vmatrix} m^2 - \xi & 1 & 2m \\ 1 & -\xi & 0 \\ m & 0 & 1 - \xi \end{vmatrix} \\ &= -(\xi + 1) \underbrace{\left(\xi^2 - m^2\xi - 2\xi + 1\right)}_{\text{irreducible Pisot polynomial}} \\ &= 0, \end{aligned} \tag{10}$$

which leads to $\xi = -1$ and $\xi_\pm = (m^2 + 2 \pm m\sqrt{m^2+4})/2$. In equation (10), $p(\xi) = \xi^2 - m^2\xi - 2\xi + 1$ is an irreducible Pisot polynomial over the field of integer numbers [31] that satisfies the PV conditions given by

$$\xi_1 > 1 \quad \text{and} \quad |\xi_l| < 1 \text{ for } 2 \le l \le S, \tag{11}$$

where S is the degree of irreducible polynomial. In other words, the 2D (m,n)-GF Labyrinth tiling with $n = 1$ fulfill the PV conditions and then, they are quasiperiodic lattices as a consequence of the quasiperiodicity of 1D (m,n)-type GF chains with $n = 1$ [28].

3 Convolution theorem for the density of states in Labyrinth tiling

Many physical properties of solids, such as the *DOS*, electric and thermal conductivities by electrons or by phonons, as well as infrared and Raman responses, can be calculated through the Green's function [32], which is determined by the Dyson equation given by $(z - \hat{H})G(z) = 1$, where $z = E + i\eta$ is a complex number, E is the energy of excitation and $\eta \to 0^+$ is the imaginary part of E [33]. For a 2D Labyrinth tiling described by Hamiltonian $\hat{H}^{\rm 2D}_{Lb}$ in equation (7), whose Green's function can be written as

$$\begin{aligned} G^{\rm 2D}_{(r,j)(k,l)}(z) &= \sum_{\alpha,\beta} \frac{\langle r \mid \alpha\rangle\langle\alpha \mid k\rangle\langle j \mid \beta\rangle\langle\beta \mid l\rangle}{z - E^{\parallel}_{\alpha}E^{\perp}_{\beta}\Big/V} \\ &= -\frac{1}{\pi}\lim_{\eta'\to 0^+}\int d\zeta \sum_{\alpha} \frac{\langle r \mid \alpha\rangle\langle\alpha \mid k\rangle}{z - E^{\parallel}_{\alpha}\zeta\Big/V} \\ &\quad \times \mathrm{Im}\left[G^{\perp}_{j,l}(\zeta + i\eta')\right], \end{aligned} \tag{12}$$

where $|\alpha\rangle|\beta\rangle$ is an eigenstate of $\hat{H}^{\rm 2D}_{Lb} = \hat{H}^{\parallel} \otimes \hat{H}^{\perp}\Big/V$ satisfying $\hat{H}^{\parallel}|\alpha\rangle = E^{\parallel}_{\alpha}|\alpha\rangle$ and $\hat{H}^{\perp}|\beta\rangle = E^{\perp}_{\beta}|\beta\rangle$, r and k are site coordinates along the x-axis, while j and l are site coordinates along the y-axis. In equation (12), we have used the following identity [33]

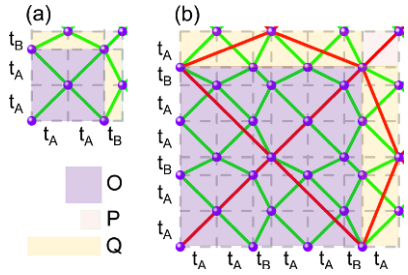

Fig. 2. Schematic representation of the 2D substitution rules of equation (9) applied to building units O (purple zone), P (green zone) and Q (yellow zone) for generations (a) two and (b) three of the silver-mean Labyrinth tiling illustrated in Figure 1a.

$$-\frac{1}{\pi}\lim_{\eta'\to 0^+}\mathrm{Im}\left[G^{\perp}_{j,l}(\zeta + i\eta')\right] = \sum_{\beta}\langle j \mid \beta\rangle\langle\beta \mid l\rangle\delta(\zeta - E^{\perp}_{\beta}). \tag{13}$$

Let us introduce a rescaled 1D Hamiltonian $\hat{H}^{\varepsilon\parallel}$ given by

$$\hat{H}^{\varepsilon\parallel}|\alpha\rangle = \varepsilon\hat{H}^{\parallel}|\alpha\rangle = \varepsilon E^{\parallel}_{\alpha}|\alpha\rangle = E^{\varepsilon\parallel}_{\alpha}|\alpha\rangle, \tag{14}$$

where $\hat{H}^{\varepsilon\parallel} = \varepsilon\hat{H}^{\parallel}$, $E^{\varepsilon\parallel}_{\alpha} = \varepsilon E^{\parallel}_{\alpha}$ and $\varepsilon = \zeta/V$. In consequence, equation (12) can be rewritten as

$$\begin{aligned} &G^{\rm 2D}_{(r,j)(k,l)}(z) \\ &\quad = -\frac{1}{\pi}\lim_{\eta'\to 0^+}\int d(\varepsilon V) G^{\varepsilon\parallel}_{r,k}(z)\mathrm{Im}\left[G^{\perp}_{j,l}(\varepsilon V + i\eta')\right], \end{aligned} \tag{15}$$

where $G^{\varepsilon\parallel}_{r,k}(z) = \sum_{\alpha}\frac{\langle r|\alpha\rangle\langle\alpha|k\rangle}{z - E^{\varepsilon\parallel}_{\alpha}}$. In general, the *DOS* is related to the Green's function through [33]

$$DOS(E) = -\frac{1}{\pi}\lim_{\eta\to 0^+}\mathrm{Im}\sum_{j} G_{j,j}(E + i\eta). \tag{16}$$

Hence, from equation (15) we obtain the convolution formula for *DOS* given by

$$DOS^{\rm 2D}(E) = \int_{-\infty}^{\infty} V d\varepsilon DOS^{\parallel}_{\varepsilon}(E) DOS^{\perp}(\varepsilon V), \tag{17}$$

where $DOS^{\parallel}_{\varepsilon}(E) = -\frac{1}{\pi}\lim_{\eta\to 0^+}\mathrm{Im}\sum_j G^{\varepsilon\parallel}_{j,j}(E + i\eta)$.

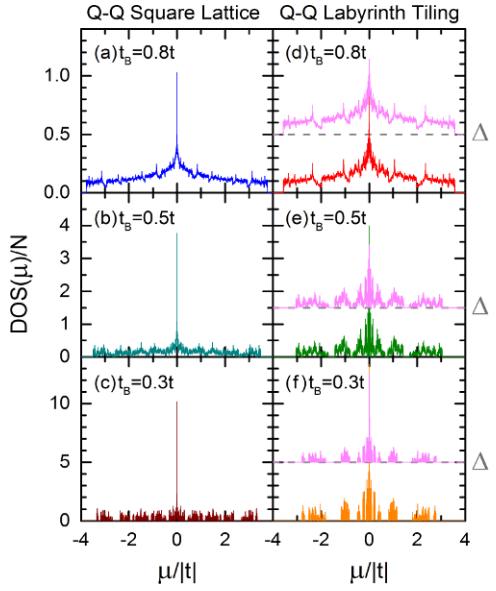

Fig. 3. Density of states (DOS) versus the chemical potential (μ) for (a–c) square and (d–f) Labyrinth tilings with a (2,1)-type GF order along both directions, denoted by Q–Q, and hopping integrals $t_A = t$ and t_B indicated in each figure. For the Labyrinth case, the DOS are compared with those reported in reference [29], whose spectra are illustrated in (d–f) with a shift Δ in the vertical direction.

Using equations (13), (15) and (16), the 2D DOS can also be expressed as

$$DOS^{2D}(E) = \frac{-1}{\pi}\sum_{\beta}\lim_{\eta\to 0^+}\mathrm{Im}\int V d\varepsilon G^{\varepsilon\parallel}_{r,r}(z) \times \sum_{j}\langle\beta \mid j\rangle\langle j \mid \beta\rangle\delta(\varepsilon V - E^{\perp}_{\beta}) = \sum_{\beta} DOS^{\parallel}_{E^{\perp}_{\beta}/V}(E), \quad (18)$$

where identities $\sum_j |j\rangle\langle j| = \mathbf{1}$ and $\langle\beta \mid \beta\rangle = 1$ were used.

The DOS of Labyrinth tiling with hopping integrals ordered following (m,n)-type GF sequences can be calculated using equations (17)–(18) and the renormalization procedure developed for GF chains of reference [26], while for corresponding square lattices this renormalization method plus convolution formulas of reference [18] are used. In Figure 3, the DOS is plotted as function of the chemical potential (μ) for (a–c) square and (d–f) Labyrinth lattices with a (2,1)-type GF quasiperiodic order along both longitudinal and transversal directions, denoted by Q–Q, containing 19 602 atoms in each direction. Both lattices along the parallel direction are connected at their ends to two semi-infinite periodic leads with null self-energies and hopping integrals t. An imaginary part of the energy $\eta = 10^{-4}|t|$, hopping integrals of (a,d) $t_B = 0.8t$, (b,e) $t_B = 0.5t$, (c,f) $t_B = 0.3t$, and (a–f) $t_A = t$ are used. In addition, the energy scale parameter is taken as $V = |t|$ along the rest of this article. In Figures 3d–3f, magenta lines illustrate the corresponding DOS reported in reference [29], whose spectra were shifted by Δ and scaled by a factor of (d) 1, (e) 2.808 and (f) 8.657 obtained from the condition $\int_{-\infty}^{\infty} DOS(E)dE = 1$. Note the excellent coincidence between both DOS spectra in each of Figures 3d–3f. Notice also the well-defined energy gaps and smaller band width in Figures 3d–3f for Labyrinth tiling in comparison with those of Figures 3a–3c, in spite of a constant coordination number of four for both square and Labyrinth lattices. It is worth mentioning that for the periodic case ($t_A = t_B = t$) both lattices have the same DOS and different conductance spectra, shown as gray spheres in Figures 4–7.

4 Electrical conductance

In this section, we analyze the electronic transport by means of the Kubo-Greenwood formula given by [33]

$$\sigma_{xx}(\mu,\omega,T) = \frac{2e^2\hbar}{\Omega\pi m^2}\frac{1}{(2i)^2}\int_{-\infty}^{\infty} dE\frac{f(E)-f(E+\hbar\omega)}{\hbar\omega} \times Tr\left[\hat{p}_x\tilde{G}(E+\hbar\omega)\hat{p}_x\tilde{G}(E)\right], \quad (19)$$

where Ω is the system volume, $\hat{p}_x = (im/\hbar)[\hat{H},\hat{x}]$ is the projection of the momentum operator along the applied electrical field, $\tilde{G}(E) = G^{+}(E) - G^{-}(E)$ is the discontinuity of Green's function, and $f(E) = \{1+\exp[(E-\mu)/k_BT]\}^{-1}$ is the Fermi-Dirac distribution with the chemical potential μ and temperature T.

Utilizing the convolution theorem demonstrated in Appendix A for the Kubo-Greenwood formula in Labyrinth tiling, whose conductivity (σ^{Lb}_{xx}) can be written as

$$\sigma^{Lb}_{xx}(\mu,\omega,T) = \frac{1}{\Omega_{\perp}}\int_{-\infty}^{\infty} V d\varepsilon\sigma^{\parallel}_{\varepsilon}(\mu,\omega,T)DOS^{\perp}(\varepsilon V), \quad (20)$$

or

$$\sigma^{Lb}_{xx}(\mu,\omega,T) = \frac{1}{\Omega_{\perp}}\sum_{\beta}\sigma^{\parallel}_{E^{\perp}_{\beta}/V}(\mu,\omega,T), \quad (21)$$

where

$$\sigma^{\parallel}_{\varepsilon}(\mu,\omega,T) = \frac{2e^2\hbar}{\Omega_{\parallel}\pi m^2}\frac{1}{(2i)^2}\int_{-\infty}^{\infty} dE\frac{f(E)-f(E+\hbar\omega)}{\hbar\omega} \times Tr\left[\hat{p}^{\varepsilon\parallel}_x\tilde{G}^{\varepsilon\parallel}(E+\hbar\omega)\hat{p}^{\varepsilon\parallel}_x\tilde{G}^{\varepsilon\parallel}(E)\right], \quad (22)$$

with $\hat{p}^{\varepsilon\parallel}_x = \varepsilon\hat{p}^{\parallel}_x$ and $\tilde{G}^{\varepsilon\parallel}(z) = G^{\varepsilon+}(z) - G^{\varepsilon-}(z)$, being $G^{\varepsilon\pm}(z) = \sum_{\alpha}|\alpha\rangle\langle\alpha|\Big/(E\pm i\eta - \varepsilon E^{\parallel}_{\alpha})$.

Equations (20) and (21) are the new convolution formulas for the Labyrinth tiling, similar to those developed for cubically structured lattices in reference [18]. In Figure 4, the electrical conductance (g) in units of $\mathrm{g}_0 = 2e^2/h$ as a function of chemical potential (μ) for (a–c) square and (d–f) Labyrinth lattices is presented. In these lattices, GF quasiperiodic sequences with $m = 1, 2,$ or 3 and $n = 1$

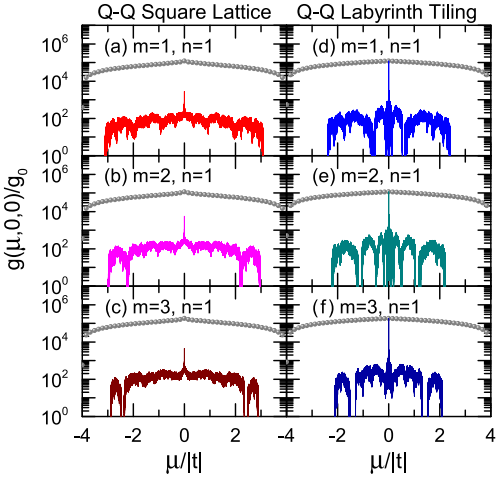

Fig. 4. Electrical conductance (g) versus the chemical potential (μ) for quasiperiodic (a–c) square and (d–f) Labyrinth lattices based on GF chains with $n = 1$ and (a,d) $m = 1$, (b,e) $m = 2$, (c,f) $m = 3$ along both directions (Q–Q), whose hopping integrals are $t_A = (\sqrt{5}-1)t/2$ and $t_B = t$, in comparison with that of the corresponding periodic square and Labyrinth lattices (gray spheres).

(indicated in each figure) were used in both longitudinal and transversal directions (Q–Q), whose lengths are specified in Table 1. The hopping integrals of these lattices are $t_A = (\sqrt{5}-1)t/2$ and $t_B = t$ with an imaginary part of the energy of $\eta = 10^{-15}|t|$.

In Figures 4a–4f, the electrical conductance spectra of corresponding periodic square and Labyrinth lattices are shown by gray spheres, where the former spectrum is obtained from [34]

$$\frac{\mathrm{g}_{xx}^{Sq}(\mu,0,0)}{\mathrm{g}_0} = \frac{\Omega_\perp}{\mathrm{g}_0\Omega_\parallel}\sigma_{xx}^{Sq}(\mu,0,0) = \frac{\Omega_\perp}{\pi}\cos^{-1}\left(\frac{|\mu|-2|t|}{2|t|}\right), \tag{23}$$

while the latter for periodic Labyrinth tiling can be analytically calculated from the convolution theorem given by equation (20) and analytical expressions of

$$\sigma^{\parallel}(\mu,0,0) = \frac{e^2\Omega_\parallel\theta(2|t|-|\mu|)}{\pi\hbar}$$
$$\text{and} \quad DOS^{\perp}(\varepsilon) = \Omega_\perp\frac{\theta(2|t|-|\varepsilon|)}{\pi\sqrt{4t^2-\varepsilon^2}}, \tag{24}$$

for periodic chains, being $\theta(\xi) = \begin{cases} 0, & \text{if } \xi < 0 \\ 1, & \text{if } \xi \geq 0 \end{cases}$. Hence, equations (20) and (24) lead to

$$\begin{aligned}\frac{\mathrm{g}_{xx}^{Lb}(\mu,0,0)}{\mathrm{g}_0} &= \frac{\Omega_\perp\sigma_{xx}^{Lb}(\mu,0,0)}{\mathrm{g}_0\Omega_\parallel} \\ &= \frac{\Omega_\perp}{\pi}\left(\int_{-2|t|}^{-|\mu|/2}\frac{d\varepsilon}{\sqrt{4t^2-\varepsilon^2}} + \int_{|\mu|/2}^{2|t|}\frac{d\varepsilon}{\sqrt{4t^2-\varepsilon^2}}\right) \\ &= \frac{2\Omega_\perp}{\pi}\cos^{-1}\left(\frac{|\mu|}{4|t|}\right). \end{aligned} \tag{25}$$

Note in Figures 4d–4f the transparent states at $\mu = 0$, whose ballistic electrical conductance scales with the system width, for Labyrinth tiling with quasiperiodic order in both longitudinal and transversal directions, denoted by Q–Q. In fact, this transparent state is present in all multidimensional Labyrinth tiling with quasiperiodic order ($n = 1$) in each direction, as a consequence of the transparent state at $\mu = 0$ in GF quasiperiodic chains [26]. An analytical proof of this fact is given in Section 5. Also, Figures 4a–4c show the electrical conductance spectra of square lattices based on the same GF quasiperiodic sequences as in Labyrinth tiling of Figures 4d–4f. Notice in Figures 4a–4c the absence of transparent states and larger band widths compared to those of the corresponding Labyrinth tiling, in which the magnitudes of hopping integrals given by equation (8) are generally smaller than those of square lattices since $|t_A| < |t|$.

Figure 5 shows the electrical conductance (g) as function of the chemical potential (μ) and system length ($N_\parallel$) along the applied electric field for (a) square and (b) Labyrinth lattices with $N_\perp = 121\,394$ for $m = n = 1$ and the same Hamiltonian parameters as in Figure 4. Notice that g generally decreases with the growth of $N_\parallel$ for both square and Labyrinth lattices. Observe in Figure 5b the appearance of transparent states at $\mu = 0$ for every 6 generations of the Labyrinth tiling, as occurred in the Fibonacci chain [26], in contrast to their absence in the corresponding square lattice.

Figure 6 shows the electrical conductance (g) versus the chemical potential (μ) for aperiodic (a–c) square and (d–f) Labyrinth lattices with $n = 2$ and (a,d) $m = 1$, (b,e) $m = 2$, and (c,f) $m = 3$ along both longitudinal and transversal directions (A–A), using the same Hamiltonian parameters as in Figure 4. The sizes of these lattices are stated in Table 1. Notice the linear scale plot of g in Figure 6, in contrast to the logarithmic one in Figure 4, which means that the g of double aperiodic lattices with $n = 2$ are generally larger than those of quasiperiodic ones with $n = 1$, except $\mu = 0$ for the Labyrinth tiling. Observe in Figure 6e the transparent state at $\mu = 0$ of the Labyrinth tiling with $m = n = 2$, and a higher g around $\mu = 0$ of Labyrinth systems in comparison with those of aperiodic square lattices.

Figure 7 illustrates spectra of g versus μ for the same (a–c) square and (d–f) Labyrinth lattices as in Figure 4, except for a periodic order with $t_A = t_B = t$ along the applied electric field direction. Such lattices are denoted by P–Q ones. Observe in their insets, Figures 7a′–7f′, the quantized steps, whose height is g_0 for square lattices and $2\mathrm{g}_0$ for Labyrinth tiling. The former is originated from the convolution formula for square lattices given by [18] $\sigma^{2\mathrm{D}}(\mu,0,0) = \sum_\beta \sigma^{\parallel}(\mu - E_\beta,0,0)\big/\Omega_\perp$ and the non-degeneracy of 1D eigenvalues (E_β), while the latter is arisen from the convolution theorem (21) for Labyrinth tiling joined with $\sigma^{\parallel}(E,0,0) = \sigma^{\parallel}(-E,0,0)$ and the mirror symmetry of non-degenerated 1D eigenvalues ($E_\beta = -E_{\beta'}$) with respect to zero in the perpendicular subspace, due to bipartite lattices along both directions. This double degeneracy of the Labyrinth tiling has been discussed in reference [29]. It is worth mentioning that

Table 1. Number of atoms in longitudinal and transversal directions of both square and Labyrinth lattices based on (m,n)-type GF chains of generation l.

	$n=1$, Quasiperiodic order (Q)		$n=2$, Aperiodic order (A)	
	Longitudinal ($\parallel$)	Transversal ($\perp$)	Longitudinal ($\parallel$)	Transversal ($\perp$)
$m=1$	433 494 438 for $l=42$	121 394 for $l=25$	178 956 972 for $l=28$	174 764 for $l=18$
$m=2$	131 836 324 for $l=22$	114 244 for $l=14$	268 377 089 for $l=20$	236 225 for $l=13$
$m=3$	790 171 310 for $l=18$	184 319 for $l=11$	253 841 390 for $l=16$	124 374 for $l=10$

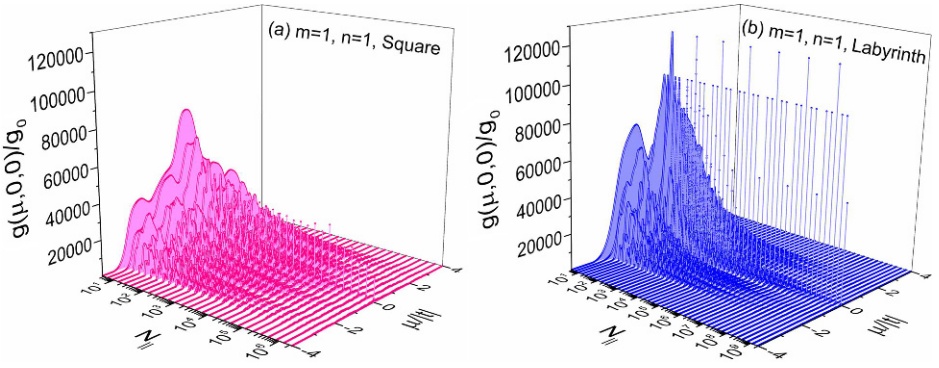

Fig. 5. Electrical conductance (g) as function of the system length ($N_\parallel$) and chemical potential (μ) for (a) square and (b) Labyrinth lattices based on GF chains with $m=n=1$, $N_\perp=121\,394$ and the same Hamiltonian parameters as in Figure 4.

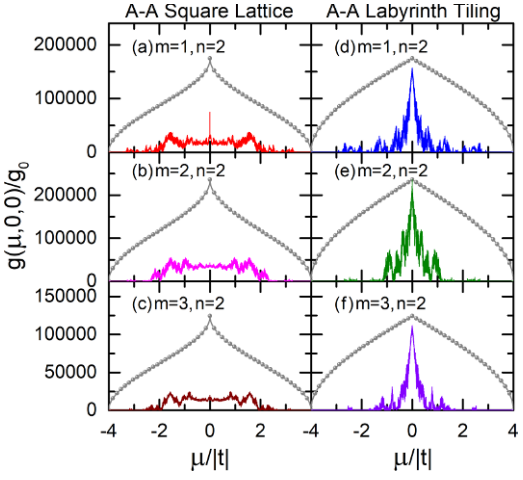

Fig. 6. Electrical conductance (g) as function of the chemical potential (μ) for aperiodic (a–c) square and (d–f) Labyrinth lattices with $n=2$ and (a,d) $m=1$, (b,e) $m=2$, (c,f) $m=3$, using the same Hamiltonian parameters of Figure 4 and comparing with the g of periodic square and Labyrinth lattices (gray spheres).

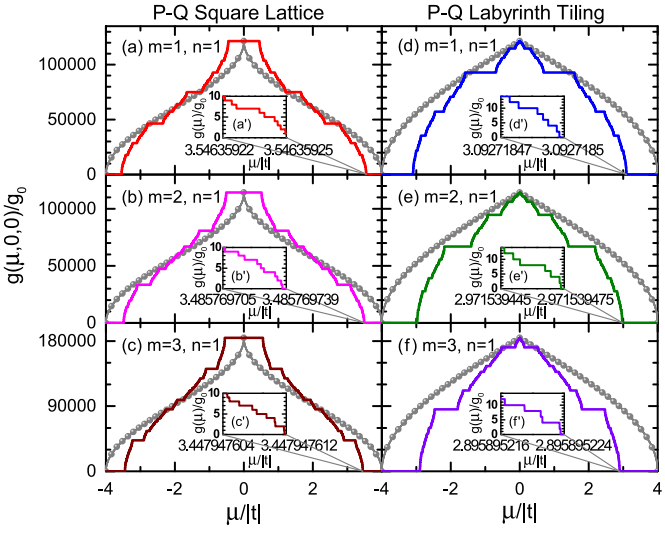

Fig. 7. Electrical conductance (g) versus the chemical potential (μ) for (a–c) square and (d–f) Labyrinth lattices with periodic-quasiperiodic (P–Q) orders along the longitudinal-transversal directions with respect to the applied electrical field. These lattices are built from GF sequences with $n=1$, $m=1,2,$ or 3 and hopping integrals $t_A=t_B=t$ along the periodic direction, while $t_B=t$ and $t_A=(\sqrt{5}-1)t/2$ along the transversal one.

these quantized heights are invariant with the change of Hamiltonian parameters. On the other hand, the integral $\int_{-\infty}^{\infty}\mathrm{g}(\mu,0,0)d\mu$ of square lattice spectra shown in Figures 7a–7c can be analytically calculated by considering that each ballistic conducting channel provides a constant area of $4\mathrm{g}_0|t|$ regardless the value of E_β and the total number of channels is the amount of atoms in the perpendicular subspace. Hence, the integrals of Figures 7a–7c for both P–P (gray spheres) and P–Q (lines) square lattices are $4N_\perp\mathrm{g}_0|t|$. For P–P Labyrinth tiling, whose conductance spectra are represented by gray spheres in Figures 7d–7f, the spectrum integral can be analytically performed by using equation (25) as $\int_{-\infty}^{\infty}\mathrm{g}(\mu,0,0)d\mu=16N_\perp\mathrm{g}_0|t|/\pi$. Now, for P–Q Labyrinth tiling in Figures 7d–7f, the conductance spectrum integrals result in $4\mathrm{g}_0\sum_\beta|E_\beta|$. In addition, given that the

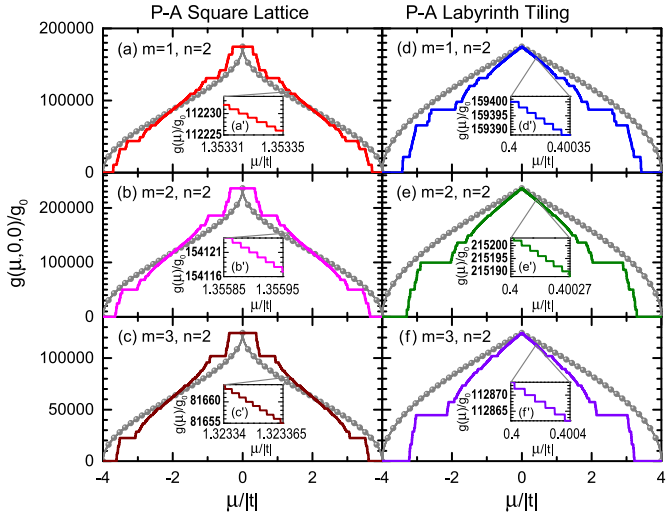

Fig. 8. Electrical conductance (g) as function of the chemical potential (μ) for square and Labyrinth lattices base on GF sequences with $n = 2$ and $m = 1, 2,$ or 3. The hopping integrals are $t_A = t$ and $t_B = t$ along the periodic (P) longitudinal direction, while $t_A = (\sqrt{5} - 1)t/2$ and $t_B = t$ in the quasiperiodic (Q) perpendicular subspace.

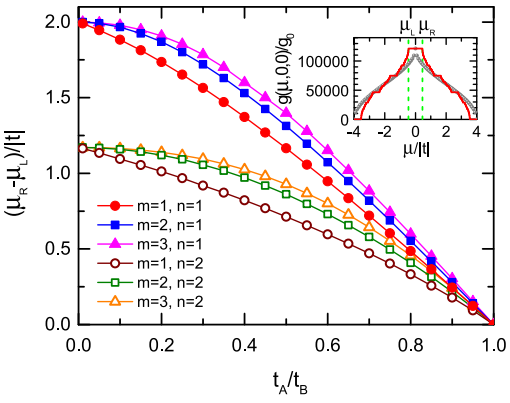

Fig. 9. Ballistic-state zone width ($\mu_R - \mu_L$) versus the hopping integral ratio (t_A/t_B) for P–Q and P–A square lattices respectively based on GF chains with $n = 1$ and $n = 2$, for $m = 1, 2,$ or 3, whose labels are indicated in the figure.

energy spectrum E_β of a Fibonacci chain with $m = 1$ and $n = 1$ constitutes a Cantor set [11], self-similar conductance spectra are found in Figures 7a and 7d for both P–Q square and Labyrinth lattices, because their quantum steps (jumps) are respectively located at $E_\beta \pm 2|t|$ and at $\pm 2E_\beta$.

Figure 8 shows the electrical conductance (g) spectra of the same systems as in Figure 7, except for $n = 2$. Observe the value of g for P–Q and P–A square lattices, respectively shown in Figures 7a–7c and 8a–8c, exceeds that of their corresponding P–P square lattices for $-2|t| < \mu < 2|t|$. In contrast, the value of g for P–Q and P–A Labyrinth tiling, correspondingly illustrated in Figures 7d–7f and 8d–8f, is generally smaller than that of their corresponding P–P Labyrinth tiling. In addition, notice the large number of ballistic conducting states with $\mathrm{g} = N_\perp \mathrm{g}_0$ around $\mu = 0$ in Figures 7a–7c and 8a–8c, respectively for P–Q and P–A square lattices. The ballistic-state zones for lattices with $n = 1$ shown in Figures 7a–7c are wider than those of lattices with $n = 2$ illustrated in Figures 8a–8c. In contrast, there is a single transparent state for Labyrinth tiling at $\mu = 0$, as occurred in P–P square and Labyrinth lattices.

In Figure 9, we present the variation of ballistic-state zone width ($\mu_R - \mu_L$) versus the hopping integral ratio (t_A/t_B) for P–Q and P–A square lattices respectively based on the GF sequences of $n = 1$ and $n = 2$, where μ_R and μ_L are respectively the right and left extreme chemical potential values of the ballistic-state zone. Notice that all the zone widths tend to zero when $t_A/t_B \to 1$, converging to the unique ballistic state of P–P square lattice. Also, for a given t_A/t_B, the zone width grows with m and diminishes when n increases. For $t_A/t_B = 0$, all these square lattices become individual ballistic channels, except those connected by t_B in the perpendicular subspace, i.e., the resulting belts have a width of $n + 1$ interconnected channels for a square lattice based on the (m,n)-type GF sequence. The eigenvalues (E_β) obtained from the perpendicular subspace of these belts determine the ballistic-state zone width, because the ballistic conduction of a square lattice at a given energy requires the ballistic transport in all individual channels and belts at this energy, i.e., the intersection of all their ballistic-state zones. For example, $E_\beta = \pm t$ for $n = 1$ and $E_\beta = 0, \pm t\sqrt{2}$ for $n = 2$, respectively lead to ballistic-state zone widths of $\mu_R - \mu_L = 2|t|$ and $\mu_R - \mu_L = 2(2 - \sqrt{2})|t|$, because such zone width ($\mu_R - \mu_L$) can be obtained from the overlap of ballistic conducting bands centered in each E_β for a given belt and a band width of $4|t|$.

5 Ballistic states in multidimensional Labyrinth tiling

In Figures 4d–4f, we observe a central state at $\mu = 0$ with ballistic signatures for Q–Q Labyrinth tiling. Actually, there is a central ballistic state every six generations for a Q–Q Labyrinth tiling based on the Fibonacci sequence with $m = n = 1$, as illustrated in Figure 5b. In this section, we present an analytical proof that this central state is truly ballistic. It would be worth emphasizing the absence of this central ballistic state in Q–Q square lattices.

Within the Landauer formalism, the 1D electrical conductivity is given by [35]

$$\sigma^{1\mathrm{D}}(\mu) = \sigma_P \mathrm{T}(\mu), \tag{26}$$

where $\sigma_P = \Omega_\parallel \mathrm{g}_0$ is the electrical conductivity of periodic chains with a system length of $\Omega_\parallel = (N_\parallel - 1)a$ and $\mathrm{T}(\mu)$ is the transmittance given by [36]

$$\mathrm{T}(\mu) = \frac{4 - (\mu/t)^2}{\left[\tau_{21} - \tau_{12} + (\tau_{22} - \tau_{11})\,\mu/2t\right]^2 + (\tau_{22} + \tau_{11})^2\left(1 - \mu^2/4t^2\right)}, \tag{27}$$

Table 2. Resulting transfer matrix for (m,n)-type GF chains of generation k.

τ	m even, n even	m even, n odd	m odd, n even	m odd, n odd
$k=2$	$(-1)^{\frac{m+n}{2}}\begin{pmatrix}0 & -1\\ 1 & 0\end{pmatrix}$	$(-1)^{\frac{m+n+1}{2}}\begin{pmatrix}1 & 0\\ 0 & 1\end{pmatrix}$	$(-1)^{\frac{m+n+1}{2}}\begin{pmatrix}\gamma & 0\\ 0 & \gamma^{-1}\end{pmatrix}$	$(-1)^{\frac{m+n}{2}}\begin{pmatrix}0 & -\gamma^{-1}\\ \gamma & 0\end{pmatrix}$
$k=3$	$(-1)^{\frac{n}{2}}\begin{pmatrix}0 & -1\\ 1 & 0\end{pmatrix}$	$(-1)^{\frac{m+n+1}{2}}\begin{pmatrix}\gamma & 0\\ 0 & \gamma^{-1}\end{pmatrix}$	$\begin{pmatrix}-\gamma & 0\\ 0 & -\gamma^{-1}\end{pmatrix}$	$(-1)^{\frac{m-1}{2}}\begin{pmatrix}\gamma^{m+1} & 0\\ 0 & \gamma^{-(m+1)}\end{pmatrix}$
$k=4$	$\begin{pmatrix}0 & -1\\ 1 & 0\end{pmatrix}$	$\begin{pmatrix}-1 & 0\\ 0 & -1\end{pmatrix}$	$(-1)^{\frac{m+n+1}{2}}\begin{pmatrix}\gamma & 0\\ 0 & \gamma^{-1}\end{pmatrix}$	$(-1)^{\frac{m+n}{2}}\begin{pmatrix}\gamma^{m-n+1} & 0\\ 0 & \gamma^{-(m-n+1)}\end{pmatrix}$
$k=5$	$\begin{pmatrix}0 & -1\\ 1 & 0\end{pmatrix}$	$\begin{pmatrix}-\gamma & 0\\ 0 & -\gamma^{-1}\end{pmatrix}$	$\begin{pmatrix}-\gamma & 0\\ 0 & -\gamma^{-1}\end{pmatrix}$	$(-1)^{\frac{m-1}{2}}\begin{pmatrix}0 & -\gamma^{n}\\ \gamma^{-n} & 0\end{pmatrix}$
$k=6$	$\begin{pmatrix}0 & -1\\ 1 & 0\end{pmatrix}$	$(-1)^{\frac{m+n+1}{2}}\begin{pmatrix}1 & 0\\ 0 & 1\end{pmatrix}$	$(-1)^{\frac{m+n+1}{2}}\begin{pmatrix}\gamma & 0\\ 0 & \gamma^{-1}\end{pmatrix}$	$\begin{pmatrix}-\gamma^{(m+1)(1-n)} & 0\\ 0 & -\gamma^{(m+1)(n-1)}\end{pmatrix}$
$k=7$	$\begin{pmatrix}0 & -1\\ 1 & 0\end{pmatrix}$	$(-1)^{\frac{m+n+1}{2}}\begin{pmatrix}\gamma & 0\\ 0 & \gamma^{-1}\end{pmatrix}$	$\begin{pmatrix}-\gamma & 0\\ 0 & -\gamma^{-1}\end{pmatrix}$	$\begin{pmatrix}-\gamma^{(m+1)(1-n)+n^2} & 0\\ 0 & -\gamma^{(m+1)(n-1)-n^2}\end{pmatrix}$
$k=8$	$\begin{pmatrix}0 & -1\\ 1 & 0\end{pmatrix}$	$\begin{pmatrix}-1 & 0\\ 0 & -1\end{pmatrix}$	$(-1)^{\frac{m+n+1}{2}}\begin{pmatrix}\gamma & 0\\ 0 & \gamma^{-1}\end{pmatrix}$	$(-1)^{\frac{m+n}{2}}\begin{pmatrix}0 & -\gamma^{-n^2}\\ \gamma^{n^2} & 0\end{pmatrix}$
$k=9$	$\begin{pmatrix}0 & -1\\ 1 & 0\end{pmatrix}$	$\begin{pmatrix}-\gamma & 0\\ 0 & -\gamma^{-1}\end{pmatrix}$	$\begin{pmatrix}-\gamma & 0\\ 0 & -\gamma^{-1}\end{pmatrix}$	$(-1)^{\frac{m-1}{2}}\begin{pmatrix}\gamma^{(m+1)(1-n+n^2)} & 0\\ 0 & \gamma^{(m+1)(n-1-n^2)}\end{pmatrix}$

being $\tau_{ij}=\left(\prod_{s=1}^{N_{\parallel}}\mathbf{M}_s\right)_{ij}$ elements of the resulting matrix (τ) obtained from the product of individual transfer matrices. Each of these transfer matrices is determined by the stationary Schrödinger equation for Hamiltonian (1) through

$$\begin{pmatrix}c_{s+1}\\ c_s\end{pmatrix}=\mathbf{M}_s\begin{pmatrix}c_s\\ c_{s-1}\end{pmatrix}=\begin{pmatrix}\mu/t_{s,s+1} & -t_{s,s-1}/t_{s,s+1}\\ 1 & 0\end{pmatrix}\begin{pmatrix}c_s\\ c_{s-1}\end{pmatrix}. \quad (28)$$

For a d-dimensional Labyrinth tiling, the electrical conductivity $(\sigma_{xx}^{d-\mathrm{D}})$ can be calculated by means of the new convolution theorem (see Appendix A) for Labyrinth tiling given by

$$\sigma_{xx}^{d-\mathrm{D}}(\mu,\omega,T)=\frac{1}{\Omega_{\perp}}\sum_{\beta}\sigma^{\parallel}_{E_{\beta}^{\perp}/V}(\mu,\omega,T), \quad (29)$$

where $\sigma^{\parallel}_{E_{\beta}^{\perp}/V}(\mu,\omega,T)$ is the rescaled electrical conductivity of the parallel subspace along the applied electric field given in equation (22) and $E_{\beta}^{\perp}$ are the eigenvalues of $(d-1)$-dimensional sub-lattice of volume $\Omega_{\perp}$ in the perpendicular subspace. For the case of direct current (DC), this rescaled 1D conductivity is related to the transmittance $\mathrm{T}(\mu)$ through equation (26) and $\mathrm{T}(\mu)$ is invariant to the rescale procedure when $\mu=0$, since the rescaling $\hat{H}^{\varepsilon\parallel}=\varepsilon\hat{H}^{\parallel}$ leaves equation (28) unchanged for $\mu=0$. In consequence, the ballistic state with $\mathrm{T}(\mu=0)=1$ in parallel sub-lattice leads to a ballistic one in multi-dimensional Labyrinth tiling.

In order to prove the existence of a ballistic state at $\mu=0$ in the parallel sub-lattice based on GF sequences, in Table 2 we present the resulting transfer matrices (τ) for the first eight generations of (m,n)-type GF chains at $\mu=0$, where $\gamma=t_A/t_B$.

The resulting transfer matrices shown in Table 2 can be summarized as follows. When m and n are both even numbers, from equation (27) we have $\mathrm{T}(\mu=0)=1$ for all generations. For the case where m is even and n is odd, the transfer matrix takes the form of

$$\tau=\left[\theta\left(\left\lfloor\frac{k}{2}\right\rfloor\right)(-1)^{(m+n+1)/2}-f\left(\left\lfloor\frac{k}{2}\right\rfloor\right)\right]\times\begin{pmatrix}\gamma^{\theta(k)} & 0\\ 0 & \gamma^{-\theta(k)}\end{pmatrix}, \quad (30)$$

where $\theta(k)=[1-(-1)^k]/2$ and $f(k)=[1+(-1)^k]/2$. Hence its transmittance is

$$\mathrm{T}(\mu=0)=\frac{4}{\left(\gamma^{\theta(k)}+\gamma^{-\theta(k)}\right)^2}, \quad (31)$$

and then, there is a ballistic state when k is an even number. On the other hand, when m is odd and n is even, the general resulting transfer matrix can be written as

$$\tau=\left[f(k)(-1)^{(m+n+1)/2}-\theta(k)\right]\begin{pmatrix}\gamma & 0\\ 0 & \gamma^{-1}\end{pmatrix}, \quad (32)$$

which leads to a transmittance of $\mathrm{T}(\mu=0)=4(\gamma+\gamma^{-1})^{-2}$ and in consequence, there is no ballistic state at $\mu=0$ for any generation. Finally, when m and n are both odd numbers, we found

$$\tau=\alpha(k)\begin{pmatrix}(1-\delta_{a,2})\gamma^{\beta(k)} & -\delta_{a,2}\gamma^{-(-1)^k n^{(k-2)/3}}\\ \delta_{a,2}\gamma^{(-1)^k n^{(k-2)/3}} & (1-\delta_{a,2})\gamma^{-\beta(k)}\end{pmatrix}, \quad (33)$$

$$T(\mu=0)=\frac{4}{\delta_{a,2}\left[\gamma^{-(-1)^k n^{(k-2)/3}}+\gamma^{(-1)^k n^{(k-2)/3}}\right]^2+(1-\delta_{a,2})\left[\gamma^{\beta(k)}+\gamma^{-\beta(k)}\right]^2}. \quad (34)$$

where $\alpha(k)=[(1-\delta_{b,0})(-1)^{(m+n)/2}-\delta_{b,0}]f(k)+[(1-\delta_{c,0})(-1)^{(m-1)/2}-\delta_{c,0}]\theta(k)$, $a=k \bmod 3 \in [0,2]$, $b=k \bmod 6 \in [0,5]$, $c=k \bmod 7 \in [0,6]$, and $\beta(k)=(m+1)\sum_{s=0}^{\lfloor k/3\rfloor-1}(-n)^s+\delta_{a,1}(-n)^{\lfloor k/3\rfloor}$. The corresponding transmittance is

See equation (34) above

Hence, there are ballistic states at $\mu=0$ for GF chains with $n=1$ and arbitrary odd numbers of m at $k=6,12,18,\ldots$ Examples of these ballistic states in Labyrinth tiling can be found in Figures 4d–4f and 6e, where numerical results confirm their presence at $\mu=0$. Furthermore, Figure 5b verifies its appearance every six generations in (1,1)-type Labyrinth tiling.

6 Conclusions

A new convolution theorem has been demonstrated for the *DOS* and Kubo-Greenwood formula in Labyrinth tiling. The numerical results of *DOS* obtained from this theorem confirm the *DOS* data of reference [29]. Such convolution theorem can be visualized as a rotation in the Hilbert space transforming a Labyrinth tiling to a set of independent chains with a rescaled 1D Hamiltonian. Let us introduce a unitary matrix ($\hat{U}^{\perp}$) that diagonalizes the Hamiltonian of perpendicular sub-space ($\hat{H}^{\perp}$), i.e., $\hat{U}^{\perp}\hat{H}^{\perp}\hat{U}^{\perp\dagger}=\hat{H}^{\perp}_{\rm diag}$. Hence, we may build a new unitary matrix given by $\hat{I}^{\parallel}\otimes\hat{U}^{\perp}$, which transforms the Hamiltonian of Labyrinth tiling $(\hat{H}^{\parallel}\otimes\hat{H}^{\perp}\big/V)$ as

$$\begin{aligned}(\hat{I}^{\parallel}\otimes\hat{U}^{\perp})\left(\frac{\hat{H}^{\parallel}\otimes\hat{H}^{\perp}}{V}\right)(\hat{I}^{\parallel}\otimes\hat{U}^{\perp})^{\dagger}&\\ =\frac{1}{V}(\hat{H}^{\parallel}\otimes\hat{U}^{\perp}\hat{H}^{\perp})(\hat{I}^{\parallel}\otimes\hat{U}^{\perp\dagger})&\\ =\frac{1}{V}\hat{H}^{\parallel}\otimes\hat{H}^{\perp}_{\rm diag}.&\end{aligned} \quad (35)$$

In other words, the original Labyrinth tiling is mapped into $N_{\perp}$ independent linear chains whose Hamiltonians are rescaled by $E^{\perp}_{\beta}\big/V$, where $N_{\perp}$ and $E^{\perp}_{\beta}$ are respectively the number of atoms and eigenvalues in the perpendicular sub-lattice.

When this convolution theorem is combined with a previously developed real-space renormalization method for the Kubo-Greenwood formula in GF chains [26], we are able to study the electronic transport in macroscopic multidimensional Labyrinth tiling based on GF sequences. Its electrical conductance is compared with that of square lattices built from the same GF chains and calculated using the traditional convolution method for cubically structured lattices [18]. When a periodic order is placed along the applied electric field direction, quantized conductance spectra are observed in both Labyrinth and square lattices, where their step heights are respectively $2\mathsf{g}_0$ and g_0. Moreover, we found a broaden ballistic state region in the square lattice case, whose extension grows with the decrease of t_A/t_B, as illustrated in Figure 9.

On the other hand, we have demonstrated the existence of a ballistic transport state at zero chemical potential ($\mu=0$) in multidimensional Labyrinth tiling based on (m,n)-type GF sequence along the applied electric field direction and any disordering lattices in the rest perpendicular directions, when (1) m and n are even numbers for all generations, (2) m is even, n is odd and the generation number k is an even number, and (3) m is odd and $n=1$ for every six generations. In summary, the reported convolution theorem permits an accurate study of the electronic transport in macroscopic multidimensional aperiodic lattices beyond cubically structured ones within the Kubo-Greenwood plus tight-binding formalism, while the analytical proof of a DC ballistic transport state in such lattices could modify the traditional correlation between periodicity and ballistic conduction. It is important to stress that this study was carried out within the single electron approximation and such ballistic transport state could be verified in a Labyrinth tiling made of low charge-carrier density materials, for example, semiconductors at low temperature.

Appendix A: Convolution theorem for Kubo-Greenwood formula in Labyrinth tiling

The electrical conductivity (σ_{xx}) can be calculated by means of the Kubo-Greenwood formula given by [33]

$$\begin{aligned}\sigma_{xx}(\mu,\omega,T)=\frac{2e^2\hbar}{\Omega\pi m^2}\frac{1}{(2i)^2}\int_{-\infty}^{\infty}dE\frac{f(E)-f(E+\hbar\omega)}{\hbar\omega}&\\ \times Tr\left[\hat{p}_x\tilde{G}(E+\hbar\omega)\hat{p}_x\tilde{G}(E)\right],&\end{aligned} \quad (A.1)$$

in which the momentum $\hat{p}_x$ in 2D Labyrinth tiling with Hamiltonian $\hat{H}=\hat{H}^{\parallel}\otimes\hat{H}^{\perp}\big/V$ is

$$\begin{aligned}\hat{p}_x^{\rm 2D}=\frac{im}{\hbar}\left(\hat{H}\hat{x}-\hat{x}\hat{H}\right)=\frac{im}{\hbar V}\Big\{(\hat{H}^{\parallel}\otimes\hat{H}^{\perp})(\hat{x}\otimes\hat{I}^{\perp})&\\ -(\hat{x}\otimes\hat{I}^{\perp})(\hat{H}^{\parallel}\otimes\hat{H}^{\perp})\Big\},&\end{aligned} \quad (A.2)$$

and using the identity of $(A\otimes B)(C\otimes D)=AC\otimes BD$, equation (A.2) becomes

$$\hat{p}_x^{2\mathrm{D}}=\frac{im}{\hbar V}\left\{(\hat{H}^{\parallel}\hat{x}-\hat{x}\hat{H}^{\parallel})\otimes\hat{H}^{\perp}\hat{I}^{\perp}\right\}=\frac{1}{V}\hat{p}_x^{\parallel}\otimes\hat{H}^{\perp}, \tag{A.3}$$

whose matrix elements are

$$\langle u,w|\hat{p}_x^{2\mathrm{D}}|r,j\rangle=p_{u,r}^{\parallel}\sum_{\beta}\frac{E_{\beta}^{\perp}}{V}\langle w\mid\beta\rangle\langle\beta\mid j\rangle, \tag{A.4}$$

where $\hat{H}^{\perp}|\beta\rangle=E_{\beta}^{\perp}|\beta\rangle$. Hence, using equation (A.4), the trace in equation (A.1) can be written as

$$\begin{aligned}
&Tr\left[\hat{p}_x^{2\mathrm{D}}\tilde{G}(z+\hbar\omega)\hat{p}_x^{2\mathrm{D}}\tilde{G}(z)\right]\\
&=\sum_{u,w}\sum_{r,j}\sum_{k,l}\sum_{f,s}\langle u,w|\hat{p}_x^{2\mathrm{D}}|r,j\rangle\langle r,j|\tilde{G}(z+\hbar\omega)|k,l\rangle\\
&\quad\times\langle k,l|\hat{p}_x^{2\mathrm{D}}|f,s\rangle\langle f,s|\tilde{G}(z)|u,w\rangle\\
&=\sum_{u,w}\sum_{r,j}\sum_{k,l}\sum_{f,s}\sum_{\gamma}\hat{p}_{u,r}^{\parallel}\frac{E_{\gamma}^{\perp}}{V}\langle w\mid\gamma\rangle\langle\gamma\mid j\rangle\tilde{G}_{(r,j)(k,l)}(z+\hbar\omega)\\
&\quad\times\sum_{\beta}\hat{p}_{k,f}^{\parallel}\frac{E_{\beta}^{\perp}}{V}\langle l\mid\beta\rangle\langle\beta\mid s\rangle\tilde{G}_{(f,s)(u,w)}(z),
\end{aligned} \tag{A.5}$$

in which $\tilde{G}(E)=G^{+}(E)-G^{-}(E)$ is the discontinuity of Green's functions and equation (12) leads to

$$\begin{aligned}
&\sum_{s,\beta}\hat{p}_{k,f}^{\parallel}\frac{E_{\beta}^{\perp}}{V}\langle l\mid\beta\rangle\langle\beta\mid s\rangle\tilde{G}_{(f,s)(u,w)}(z)\\
&\quad=\sum_{s,\beta}\hat{p}_{k,f}^{\parallel}\frac{E_{\beta}^{\perp}}{V}\langle l\mid\beta\rangle\langle\beta\mid s\rangle\\
&\qquad\times\left[G_{(f,s)(u,w)}^{+}(z)-G_{(f,s)(u,w)}^{-}(z)\right]\\
&\quad=\sum_{s,\beta}\hat{p}_{k,f}^{\parallel}\frac{E_{\beta}^{\perp}}{V}\langle l\mid\beta\rangle\langle\beta\mid s\rangle\\
&\qquad\times\left(\sum_{\alpha,\gamma}\frac{\langle f\mid\alpha\rangle\langle\alpha\mid u\rangle\langle s\mid\gamma\rangle\langle\gamma\mid w\rangle}{z-E_{\alpha}^{\parallel}E_{\gamma}^{\perp}\big/V}\right.\\
&\qquad\left.-\sum_{\alpha,\gamma}\frac{\langle f\mid\alpha\rangle\langle\alpha\mid u\rangle\langle s\mid\gamma\rangle\langle\gamma\mid w\rangle}{z^{*}-E_{\alpha}^{\parallel}E_{\gamma}^{\perp}\big/V}\right)\\
&\quad=\int Vd\varepsilon\hat{p}_{k,f}^{\parallel}\varepsilon\sum_{\alpha}\left(\frac{\langle f\mid\alpha\rangle\langle\alpha\mid u\rangle}{z-\varepsilon E_{\alpha}^{\parallel}}-\frac{\langle f\mid\alpha\rangle\langle\alpha\mid u\rangle}{z^{*}-\varepsilon E_{\alpha}^{\parallel}}\right)\\
&\qquad\times\sum_{\beta}\langle l\mid\beta\rangle\langle\beta\mid w\rangle\delta(\varepsilon V-E_{\beta}^{\perp}).
\end{aligned} \tag{A.6}$$

From Hamiltonian $\hat{H}^{\varepsilon\parallel}$ of equation (14), the rescaled momentum is given by

$$\hat{p}_x^{\varepsilon\parallel}=\frac{im}{\hbar}[\hat{x},\hat{H}^{\varepsilon\parallel}]=\varepsilon\frac{im}{\hbar}[\hat{x},\hat{H}^{\parallel}]=\varepsilon\hat{p}_x^{\parallel}, \tag{A.7}$$

and equation (A.6) becomes

$$\begin{aligned}
&\sum_{s,\beta}\hat{p}_{k,f}^{\parallel}\frac{E_{\beta}^{\perp}}{V}\langle l\mid\beta\rangle\langle\beta\mid s\rangle\tilde{G}_{(f,s)(u,w)}(z)\\
&\quad=\int Vd\varepsilon\hat{p}_{k,f}^{\varepsilon\parallel}\sum_{\alpha}\left(\frac{\langle f\mid\alpha\rangle\langle\alpha\mid u\rangle}{z-E_{\alpha}^{\varepsilon\parallel}}-\frac{\langle f\mid\alpha\rangle\langle\alpha\mid u\rangle}{z^{*}-E_{\alpha}^{\varepsilon\parallel}}\right)\\
&\qquad\times\sum_{\beta}\langle l\mid\beta\rangle\langle\beta\mid w\rangle\delta(\varepsilon V-E_{\beta}^{\perp})\\
&\quad=\int Vd\varepsilon\hat{p}_{k,f}^{\varepsilon\parallel}\tilde{G}_{f,u}^{\varepsilon\parallel}(z)\sum_{\beta}\langle l\mid\beta\rangle\langle\beta\mid w\rangle\delta(\varepsilon V-E_{\beta}^{\perp}),
\end{aligned} \tag{A.8}$$

where $\tilde{G}^{\varepsilon\parallel}(z)=G^{\varepsilon+}(z)-G^{\varepsilon-}(z)$ and $G^{\varepsilon\pm}(z)=\sum_{\alpha}|\alpha\rangle\langle\alpha|\big/(E\pm i\eta-E_{\alpha}^{\varepsilon\parallel})$. Hence, the trace of equation (A.5) can be rewritten as

$$\begin{aligned}
&Tr\left[\hat{p}_x^{2\mathrm{D}}\tilde{G}(z+\hbar\omega)\hat{p}_x^{2\mathrm{D}}\tilde{G}(z)\right]\\
&\quad=\sum_{u,w}\sum_{r}\sum_{k,l}\sum_{f}\int Vd\varepsilon'\hat{p}_{u,r}^{\varepsilon'\parallel}\tilde{G}_{r,k}^{\varepsilon'\parallel}(z+\hbar\omega)\\
&\qquad\times\sum_{\gamma}\langle w\mid\gamma\rangle\langle\gamma\mid l\rangle\delta(\varepsilon'V-E_{\gamma}^{\perp})\\
&\qquad\times\int Vd\varepsilon\hat{p}_{k,f}^{\varepsilon\parallel}\tilde{G}_{f,u}^{\varepsilon\parallel}(z)\sum_{\beta}\langle l\mid\beta\rangle\langle\beta\mid w\rangle\delta(\varepsilon V-E_{\beta}^{\perp})\\
&\quad=\int Vd\varepsilon\sum_{u,r,k,f}\hat{p}_{u,r}^{\varepsilon\parallel}\tilde{G}_{r,k}^{\varepsilon\parallel}(z+\hbar\omega)\hat{p}_{k,f}^{\varepsilon\parallel}\tilde{G}_{f,u}^{\varepsilon\parallel}(z)\\
&\qquad\times\sum_{\beta,w}\langle w\mid\beta\rangle\langle\beta\mid w\rangle\delta(\varepsilon V-E_{\beta}^{\perp})\\
&\quad=\int Vd\varepsilon Tr\left[\hat{p}_x^{\varepsilon\parallel}\tilde{G}^{\varepsilon\parallel}(z+\hbar\omega)\hat{p}_x^{\varepsilon\parallel}\tilde{G}^{\varepsilon\parallel}(z)\right]\\
&\qquad\times\sum_{\beta,w}\langle w\mid\beta\rangle\langle\beta\mid w\rangle\delta(\varepsilon V-E_{\beta}^{\perp}),
\end{aligned} \tag{A.9}$$

where $\sum_{l}|l\rangle\langle l|=1$ and $\langle\gamma\mid\beta\rangle=\delta_{\gamma,\beta}$ were used. Therefore, the new convolution theorem for Kubo-Greenwood formula (A.1) in Labyrinth tiling can be expressed as

$$\sigma_{xx}^{Lb}(\mu,\omega,T)=\frac{1}{\Omega_{\perp}}\int_{-\infty}^{\infty}Vd\varepsilon\sigma_{\varepsilon}^{\parallel}(\mu,\omega,T)DOS^{\perp}(\varepsilon V) \tag{A.10}$$

or

$$\sigma_{xx}^{Lb}(\mu,\omega,T)=\frac{1}{\Omega_{\perp}}\sum_{\beta}\sigma_{E_{\beta}^{\perp}/V}^{\parallel}(\mu,\omega,T), \tag{A.11}$$

where $\sigma_{\varepsilon}^{\parallel}(\mu,\omega,T)=\frac{2e^2\hbar}{\Omega_{\parallel}\pi m^2}\frac{1}{(2i)^2}\int_{-\infty}^{\infty}dE\frac{f(E)-f(E+\hbar\omega)}{\hbar\omega}Tr\left[\hat{p}_x^{\varepsilon\parallel}\tilde{G}^{\varepsilon\parallel}(E+\hbar\omega)\hat{p}_x^{\varepsilon\parallel}\tilde{G}^{\varepsilon\parallel}(E)\right]$.

This work has been partially supported by the Consejo Nacional de Ciencia y Tecnología of Mexico through grant 252943 and by the National Autonomous University of Mexico

through projects PAPIIT-IN114916 and PAPIIT-IN116317. Computations were performed at Miztli of DGTIC-UNAM.

Author contribution statement

All the authors were involved in the design and development of the present research, as well as in the manuscript preparation.

References

1. N.W. Ashcroft, N.D. Mermin, *Solid state physics* (Harcourt College Publishers, Fort Worth, 1976)
2. E. Abrahams, P.W. Anderson, D.C. Licciardello, T.V. Ramakrishnan, Phys. Rev. Lett. **42**, 673 (1979)
3. D. Shechtman, I. Blech, D. Gratias, J.W. Cahn, Phys. Rev. Lett. **53**, 1951 (1984)
4. E. Maciá, ISRN Condens. Matter Phys. **2014**, 165943 (2014)
5. M. Renner, G. Von Freymann, Sci. Rep. **5**, 13129 (2015)
6. M. Hollander, B. Solomyak, Ergod. Theory Dyn. Syst. **23**, 533 (2003)
7. J. Kellendonk et al. (Eds.) *Mathematics of aperiodic order* (Springer, Heidelberg, 2015)
8. M. Kohmoto, Phys. Rev. Lett. **51**, 1198 (1983)
9. N. Macé, A. Jagannathan, F. Piéchon, Phys. Rev. B **93**, 205153 (2016)
10. E. Maciá, *Aperiodic structures in condensed matter: fundamentals and applications* (CRC Press, Boca Raton, 2009)
11. D. Damanik, A. Gorodetski, W. Yensse, Invent. Math. **206**, 629 (2016)
12. E.L. Albuquerque, M.G. Cottam, Phys. Rep. **376**, 225 (2003)
13. C. Huang, F. Ye, X. Chen, Y.V. Kartashov, V.V. Konotop, L. Torner, Sci. Rep. **6**, 32546 (2016)
14. I.F. Herrera-González, J.A. Méndez-Bermúdez, F.M. Izrailev, Phys. Rev. E **90**, 042115 (2014)
15. G. Trambly de Laissardière, C. Oguey, D. Mayou, J. Phys.: Conf. Ser. **809**, 012020 (2017)
16. Z. Akdeniz, P. Vignolo, Physica E **91**, 136 (2017)
17. R.J. Lifshitz, Alloys Compd. **342**, 186 (2002)
18. V. Sánchez, C. Wang, Phys. Rev. B **70**, 144207 (2004)
19. C. Sire, Europhys. Lett. **10**, 483 (1989)
20. V.Z. Cerovski, M. Schreiber, U. Grimm, Phys. Rev. B **72**, 054203 (2005)
21. S. Thiem, M. Schreiber, J. Phys.: Conf. Ser. **226**, 012029 (2010)
22. S. Thiem, M. Schreiber, J. Phys.: Condens. Matter **25**, 075503 (2013)
23. S. Thiem, M. Schreiber, Phys. Rev. B **85**, 224205 (2012)
24. G.Y. Oh, M.H. Lee, Phys. Rev. B **48**, 12465 (1993)
25. X. Fu, Y. Liu, Z. Guo, P. Zhou, X. Huang, Phys. Rev. B **51**, 3910 (1995)
26. F. Sánchez, V. Sánchez, C. Wang, J. Noncryst. Solids **450**, 194 (2016)
27. E. Maciá, Rep. Prog. Phys. **75**, 036502 (2012)
28. T. Takahashi, J. Math. Phys. **57**, 063506 (2016)
29. H.Q. Yuan, U. Grimm, P. Repetowicz, M. Schreiber, Phys. Rev. B **62**, 15569 (2000)
30. Y. Takahashi, Nonlinearity **30**, 2114 (2017)
31. R. Lidl, H. Niederreiter, *Introduction to finite fields and their applications* (Cambridge University Press, London, 1986)
32. R.J. Elliott, J.A. Krumhansl, P.L. Leath, Rev. Mod. Phys. **46**, 465 (1974)
33. E.N. Economou, *Green's functions in quantum physics*, 3rd edn. (Springer, Berlin, 2006)
34. V. Sánchez, C. Wang, J. Alloys Compd. **342**, 410 (2002)
35. R. Landauer, Philos. Mag. **21**, 863 (1970)
36. R. Oviedo-Roa, L.A. Pérez, C. Wang, Phys. Rev. B **62**, 13805 (2000)